

# Optical pH Detection within a Protein Crystal

Klaus M. Seemann,<sup>\*,†,‡</sup> Reiner Kiefersauer,<sup>‡,§,#</sup> Uwe Jacob,<sup>§,‡</sup> and Bernd Kuhn<sup>\*,||,⊥,‡</sup>

<sup>†</sup>Peter Grünberg Institute, Research Center Jülich, 52425 Jülich, Germany

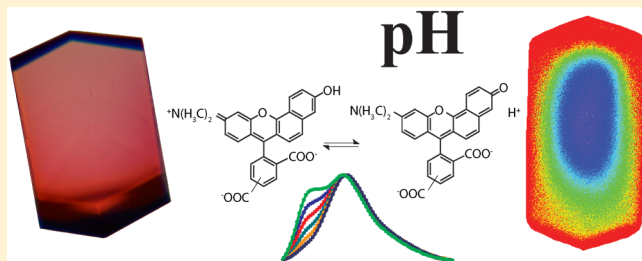
<sup>‡</sup>Proteros biostructures GmbH, 82152 Martinsried, Germany

<sup>§</sup>Westend-Innovation GmbH, 80339 München, Germany

<sup>||</sup>Department of Membrane and Neurophysics, Max Planck Institute of Biochemistry, 82152 Martinsried, Germany

<sup>⊥</sup>Optical Neuroimaging Unit, Okinawa Institute of Science and Technology Graduate University, Onna-son, Okinawa 904-0412, Japan

**ABSTRACT:** The pH is one of the key parameters governing protein conformation and activity. In protein crystals, however, the pH is so far not accessible by experiment. Here, we report on the optical detection of the pH in a lysozyme crystal employing the pH-sensitive fluorescent dyes SNARF-1 and SNARF-4F. The molecular probes were loaded into the crystal by diffusion. Two-dimensional fluorescence spectra of the labeled protein crystal were recorded, and the average pH of the crystal at different bath pH's was determined by calibrating fluorescence peak ratios. In addition, we used two-photon microscopy to spatially resolve the pH inside a lysozyme crystal three-dimensionally and to follow pH changes in response to a pH change of the bath over time. At equilibrium at bath pH between 5.5 and 8.0, we found a pH in the water-filled crystal channels that was  $\Delta\text{pH} = -0.3$  to  $-1.0$  lower than that of the bath. This corresponds to a 2- to 10-fold higher proton concentration in the crystal channels than in the bath. The lower pH at equilibrium in the crystal channels can be explained by slower proton diffusion in the channels than in the bath and a resulting proton accumulation in the crystal for conservation of mass and so an equilibrium of proton flux.



## INTRODUCTION

Protein structures obtained from diffraction patterns of crystals are the basis of our structural and mechanistic understanding of biology. Since the pH strongly influences protein conformation, it is important to consider the pH during the diffraction. It would be also very interesting to specifically change the pH in the crystal in a defined way to study pH-dependent mechanisms and to acquire structures at physiological pH. Therefore, pH measurement within the protein crystal would be a very useful tool.

The protein most widely used as a model in crystallography is hen egg-white lysozyme,<sup>1</sup> as it can be easily purified in large quantities and readily crystallized. Importantly for this project, lysozyme has been extensively studied in the past in terms of its structure,<sup>1</sup> pH-dependent folding and unfolding kinetics,<sup>2–5</sup> water diffusion,<sup>6,7</sup> and proton diffusion.<sup>6</sup> Lysozyme crystals are known to have 1 nm wide water-filled channels and a water concentration of 20 mol/L,<sup>1,7</sup> corresponding to 36% of the crystal volume. The sodium chloride/acetate buffer solution, in which the crystals are grown, constitutes about 33.5% of the crystal weight.<sup>1</sup> Such large water content with buffer assures a defined pH in the protein crystal.

The demand for pH measurements in biology has led to the development of pH-sensitive fluorescent probes.<sup>8–10</sup> These probes are proton buffers, and their absorption and/or fluorescence characteristic changes upon protonation and

deprotonation. Especially rhodamine-based pH indicators have attracted attention due to high quantum yield and two clearly distinguishable emission bands.<sup>11</sup> Double emission is particularly useful, as it allows evaluation of pH via a ratio of intensities and so eliminates concentration dependence.

Two fluorescent pH probes with dual emission spectra are 5'-(and 6')-carboxy-10-dimethylamino-3-hydroxy-spiro(7H-benzo(c)xanthene-7,1'(3'H-isobenzofuran)-3'-one (SNARF-1)<sup>11</sup> and 1,4-(and 5)-benzenedicarboxylic acid, 2-[10-(dimethylamino)-4-fluoro-3-oxo-3H-benzo[c]xanthene-7-yl] (SNARF-4F).<sup>12</sup> Both dyes have been extensively used to determine the pH in biological specimens.<sup>10,13–17</sup> However, care has to be taken, as there are several mechanisms that can deteriorate the optical pH measurement. Interaction of SNARF-1 with other chemical compounds present in solution,<sup>18</sup> the effect of photobleaching,<sup>15</sup> or quenching<sup>19</sup> have been reported to change fluorescence and/or dissociation constant  $K_a$ .<sup>20</sup> So far, no SNARF-1/protein interactions were found in cells,<sup>18</sup> however, the fluorescence characteristic changed dramatically when in solution with the transporter protein BSA.<sup>19</sup> In general, pH sensitive dyes are expected to be sensitive to the local molecular environment.<sup>21</sup>

Received: October 27, 2011

Revised: July 24, 2012

Published: July 27, 2012

There are mainly two possibilities to read out the pH of these molecular probes. Fluorescence can be detected spectrally resolved by spectrometers. This allows a precise spectral analysis and is also used to determine the functionality of a probe. Alternatively, fluorescence can be detected spatially resolved and pH maps can be acquired. This is mainly done by wide field fluorescence microscopy or confocal microscopy. In confocal microscopy, a focused laser beam is scanned through the sample to excite fluorescence, while a spatial pinhole is used to selectively pass photons for detection coming from the direction of the focal spot and to block all other photons from reaching the detector. This allows sectioning and so three-dimensional reconstruction of the sample. In scattering samples like biological tissue, however, two-photon microscopy<sup>22,23</sup> has several advantages over confocal microscopy. In two-photon microscopy, a focused, pulsed infrared laser beam is scanned through a transparent sample. Fluorescent dye molecules cannot be excited by a single infrared photon, as the energy is too low for transition into an excited electronic state. However, simultaneous, i.e., within Heisenberg's uncertainty principle, absorption of two or more photons, which then add up their energy, can excite the molecule. The probability for this process is nonlinearly increasing with the excitation light intensity. The laser intensity is chosen so that excitation occurs only in the focal spot which is under optimal conditions  $0.2 \times 0.2 \times 0.6 \mu\text{m}^3$  (fwhm). Therefore, two-photon microscopy allows sectioning, eliminates out-of-focus excitation, and so reduces photochemical effects such as phototoxicity and bleaching. These advantages make two-photon microscopy the method of choice not only for imaging of living specimens but also for spatially resolved, optical pH detection in crystals.

In this work, we applied SNARF-1 and SNARF-4F for the pH measurement within lysozyme crystals. At first, we analyzed the interaction of the dye with the protein crystal to test the viability of the approach. Then, we measured the fluorescence of SNARF-1 labeled crystals spectrally resolved in excitation and emission with a diode array spectrometer and a monochromator for excitation, both coupled to a microscope. The fluorescence ratios were calibrated to determine the average pH of the crystal. Furthermore, we imaged the pH spatially resolved with SNARF-1 and SNARF-4F and pH changes spatially and temporally resolved with SNARF-1 using two-photon microscopy. We can explain our results by differences of the proton diffusion coefficients in the bath and crystal and a balanced flux of protons.

## MATERIALS AND METHODS

**Crystallization.** Lysozyme is a hydrolase enzyme consisting of 129 amino acid residues and has a molecular weight of approximately 14.7 kDa. Lyophilized, salt free hen egg-white lysozyme (Serva and Sigma) was brought into 50 mM acetate buffer solution (pH 4.5) and filtered to remove excess crystallization nuclei. The sitting-drop method using 1 M sodium chloride and 50 mM acetate buffer, pH 4.5, as precipitant at 20 °C resulted in protein crystals reaching typical sizes of 200–500 μm within 3 days.

**Crystal Labeling.** Stock solutions of the pH-sensitive dual emission fluorescent dyes 5'-(6')-carboxy-10-dimethylamino-3-hydroxy-spiro[7H-benzo[c]xanthene-7,1'(3'H)-isobenzofuran]-3'-one (SNARF-1, Molecular Probes, MW453, pK<sub>a</sub> 7.5) or 1,4-(and 5)-benzenedicarboxylic acid, 2-[10-(dimethylamino)-4-fluoro-3-oxo-3H-benzo[c]xanthen-7-yl] (SNARF-4F, Molecular Probes, MW471, pK<sub>a</sub> 6.4) were prepared at concentrations

of 5 and 2.5 mM, respectively, in water. The stock solutions were diluted in precipitant to 200 or 1 μM and then added at a ratio of 1:1 to the native crystallization solution (10 μL) so that the final dye concentration was 100 or 0.5 μM in a 20 μL volume with 12.5 mg/mL lysozyme. The dyes were allowed to diffuse into the lysozyme crystals for more than 72 h.

**Crystal Delabeling.** For optimal delabeling, a single SNARF-1-labeled crystal was placed onto a raised platform within 1 L of 1.2 M sodium chloride solution with 50 mM acetate buffer, pH 4.5, with constant but gentle magnetic stirring. Crystals were imaged every 24 h. An exponential decay curve was fitted to determine the time constant  $\tau$  of delabeling and to test for trapped dye.

**Crystal pH Change.** pH changes of the crystal were performed in steps of ΔpH = 0.25 every 5 min by exchanging bath solutions containing 1.2 M sodium chloride and 50 mM acetate buffer (pH 4.5–6.5) or 50 mM Tris buffer (pH 6.5–8.0) at 25 °C, titrated with HCl or NaOH. The pH of solutions was calibrated with pH meters (PHM62, Radiometer Copenhagen, and F-52, Horiba). At least 90 min were needed to equilibrate the crystal pH. In general, mechanical and osmotic stress was carefully avoided, as it easily causes cracks in the crystal.

For imaging the time course of crystal pH change, the bath solution of a crystal in equilibrium with a 1.2 M NaCl and 50 mM acetate solution, pH 6.0, was exchanged to a 1.2 M NaCl and 50 mM Tris solution, pH 7.5, within 5 min. Imaging started 10 min after the beginning of the exchange procedure.

**X-ray Structure.** In the diffraction experiment, we used a monochromated Cu Kα line of a Rigaku X-ray tube operated at 50 kV and 100 mA anode current in combination with an image-plate system to record the diffractions of the protein crystal permitting a maximal electron density resolution of 2.012 Å. The tetragonal lysozyme crystal was indexed by the P4<sub>3</sub>2<sub>1</sub>2 space group. The crystal was labeled with 100 μM SNARF-1 in bath solution.

**Gel Electrophoresis.** For gel electrophoresis experiments, lysozyme in concentrations ranging from 1 to 30 mg/mL was dissolved in 50 mM Tris buffer solution containing 1 M sodium chloride and 0.1 mM SNARF-1. The SDS pages were at first examined in UV light to see the fluorescence of the SNARF-1 bands and then stained with coomassie blue to make lysozyme visible.

**Crystal Image.** The crystal image was taken in transmitted light of a condenser (Olympus) with a 5×/N.A.0.25 objective (Fluar, Zeiss), a 200 mm tube lens (Thorlabs), and a SLR camera (D7000, Nikon). The image is white point corrected to reproduce the color correctly. The crystal was labeled with 100 μM SNARF-1 in the bath solution.

**Spectrometry.** Crystal pH measurements were done in 1.2 M sodium chloride solution buffered with 50 mM Tris free of fluorescent dye. The emission maxima of the protonated and deprotonated SNARF-1 are at wavelengths of  $\lambda_a = 595$  nm and  $\lambda_b = 640$  nm, respectively.

For the spectroscopic measurements, a microscope-coupled 2-dimensional fluorescence spectrometer was used and the data was calibrated to quantum spectra as described before.<sup>24</sup> In short, to record two-dimensional fluorescence spectra, a monochromator illuminated by a Xenon lamp (J&M Analytik AG, Aalen, Germany) was coupled to an inverted fluorescence microscope (Zeiss Axiovert) with immersion objective (Neofluar 100×/1.3 oil, Zeiss). The fluorescence was detected by a 256-diode array spectrometer with an average spectral

resolution of 3.1 nm (J&M Analytik AG). A dichroic mirror (515 nm, Chroma) and a long-pass filter (520 nm, Chroma) were used to separate excitation and emission. The excitation wavelength was varied between 400 and 510 nm in steps of 5 nm. The integration time of the detector was 1000 ms at each excitation wavelength setting. Two-dimensional fluorescence spectra were acquired with the focal plane within the crystal. To avoid any residual fluorescence from the bath, the excitation area was adapted by the microscope field stop to the size of the crystal. The field stop can be closed to a field of excitation of about 5  $\mu\text{m}$  diameter defining the maximal spatial resolution of the measurement.

The spectra of the dye in buffer solution were used to generate a pH calibration curve by fitting

$$\frac{I_b - I_{b0}}{I_a - I_{a0}} \propto \frac{[\text{SNARF}^- \text{H}^+]}{[\text{SNARF}^-]} = \frac{[\text{H}^+]}{K_a}$$

where  $I$  is the intensity at the two fluorescence maxima at  $\lambda_a$  and  $\lambda_b$ ,  $I_0$  the corresponding baseline fluorescence intensity,  $[\text{SNARF}^-]$  and  $[\text{SNARF}^- \text{H}^+]$  indicate concentrations of deprotonated and protonated dye, and  $K_a$  denotes the dissociation constant of the dye.

**Two-Photon Microscopy.** We used a custom built two-photon microscope (MOM, Sutter) based on the design of Winfried Denk and running ScanImage<sup>25</sup> software. An ultrafast Ti:sapphire laser (Vision II, Coherent) for excitation, a 20 $\times$ /1.0 N.A. water immersion objective (Zeiss), and two GaAsP photomultiplier tubes (Hamamatsu) for fluorescence detection were used. Fluorescence was detected simultaneously in the orange (565–595 nm bandpass filter, Chroma) and red (635–685 nm bandpass filter, Chroma) wavelength range separated by a 610 nm dichroic mirror (Chroma). We tested excitation at 800, 900, 1000, and 1080 nm and found similar pH sensitivity (slope of calibration curve). We used 1000 nm for SNARF-1 and SNARF-4F excitation, as the orange to red ratio was lowest and closest to 1 in the range between pH 7.0 and 8.0 and pH 5.5 and 6.5, respectively.

The crystal measurements were done in dye-free 1.2 M sodium chloride and 50 mM Tris buffer in a 400  $\mu\text{m}$  thick closed chamber built from glass coverslips, slides, and dental acrylic. To improve the reopening of the chambers and reduce leakage, the chambers were made hydrophobic in 5% dichlorodimethylsilane (Wacker) in toluene. Stacks for three-dimensional reconstruction of the crystals were acquired with 512 by 512 pixels, at 2 ms per line, 5  $\mu\text{m}$  z-steps, and 4, 9, or 16 averages. The laser power typically used for reconstructing crystals was in the range of 10 mW, and up to 50 mW for time course measurements. Background levels  $B$  of the orange and red channel were acquired with the laser shutter closed. To calculate lines of fluorescence ratios  $R(x)$  through the crystal, the intensities  $I$  were background corrected by subtracting  $B$  and summed over a range of slices  $z$  and rows  $y$  before calculating the ratio.

$$R(x) = \frac{\sum_{z=k}^{k+n} \sum_{y=l}^{l+m} (I_{\text{red},y,z}(x) - B_{\text{red}})}{\sum_{z=k}^{k+n} \sum_{y=l}^{l+m} (I_{\text{orange},y,z}(x) - B_{\text{orange}})}$$

This averaging was done to improve the signal-to-noise ratio. The range of average in  $z$  and  $y$  direction is indicated in Figures 5 and 6 by the shaded areas.

For calibration, the laser was focused 10  $\mu\text{m}$  into a 100  $\mu\text{M}$  SNARF-1 or SNARF-4F solution in 1.2 M sodium chloride and

50 mM Tris or acetate buffer titrated to different pH's by HCl or NaOH.

Data was analyzed with IgorPro (WaveMetrics) and ImageJ (National Institute of Health).

**Imaging of Crystal Labeling.** To image the time course of labeling, 1 mm thick chambers were built from glass slides and glass coverslips and glued with dental acrylic. The crystals were put in the chambers with 500  $\mu\text{L}$  of 500 nM SNARF-1 in 1.2 M NaCl and 50 mM acetate buffer, pH 4.5, and sealed to allow long-term imaging. The crystals were regularly 3D reconstructed. To analyze the fluorescence intensity in the crystal, the signals of the orange and red channels were added to reduce the effect of pH on the intensity. Additionally, close to pH 4.5, pH-induced intensity changes of SNARF-1 are small. The SNARF-1 diffusion coefficient  $D$  was calculated from

$$\langle x^2 \rangle = 4Dt$$

where  $x$  is the distance from the crystal surface to where the normalized fluorescence intensity has decreased to  $1/e$  and  $t$  is the time after addition of dye to the bath and crystal.

## RESULTS AND DISCUSSION

**Labeling of Lysozyme Crystals with SNARF-1.** We used crystalline lysozyme (Figure 1a) as a model matrix. To analyze the labeling process, we added SNARF-1 (Figure 1b) to the bath and imaged the time course of dye diffusing into the crystal (Figure 1c,d). The time course reveals a diffusion coefficient  $D_{\text{S1 crystal channel}}$  of  $3.4 \times 10^{-3} \pm 1.0 \times 10^{-3} \mu\text{m}^2/\text{s}$  which is about  $10^5$ -fold lower than diffusion of similar rhodamine dyes in water ( $400 \mu\text{m}^2/\text{s}$ ).<sup>26</sup> This slow diffusion is plausible because of the only about 1 nm wide water-filled channels in the lysozyme crystal.<sup>7</sup>

In equilibrium after more than 72 h, assuming similar fluorescence characteristics in the crystal as in the bath, we found an intensity increase in the crystal of about 275 times compared to the bath. As the dye diffuses only in the channels of the crystal, the dye concentration in the channels was even 760 times higher. A 100  $\mu\text{M}$  SNARF-1 bath solution resulted in a dye concentration of 27.5 mM in the crystal (Figure 1a). Such concentration is in the range of the lysozyme concentration in the crystal (56 mM),<sup>1</sup> and so the dye is contributing to some extent to the pH buffering in the crystal channels.

The difference in diffusion coefficient can be used to explain the high accumulation of dye in the crystal. In equilibrium, the flux of dye into and out of the crystal has to be equal and so the concentration  $[\text{SNARF-1}]_{\text{crystal channel}}$  compensates for the slower diffusion in the crystal

$$\begin{aligned} & \frac{A_{\text{open}}}{A_{\text{total}}} D_{\text{S1 bath}} [\text{SNARF-1}]_{\text{bath}} \\ &= D_{\text{S1 crystal channel}} [\text{SNARF-1}]_{\text{crystal channel}} \end{aligned}$$

We introduce a correction factor to account for the fraction of open surface area  $A_{\text{open}}$  to the total surface  $A_{\text{total}}$  of the crystal which is in a first approximation 0.36.<sup>1</sup> On the basis of the data of our experiments, this equation suggests that the SNARF-1 diffusion in 1.2 M NaCl and 50 mM acetate buffer is reduced to  $7.2 \mu\text{m}^2/\text{s}$ . A reduction of dye diffusion is plausible because of the high osmolarity (2450 mOsmol) of the bath solution. Previous experiments, however, did not find a dependence of the diffusion constant of rhodamine on ionic strength,<sup>26</sup> but the tested range was more than 2 orders of magnitude lower than

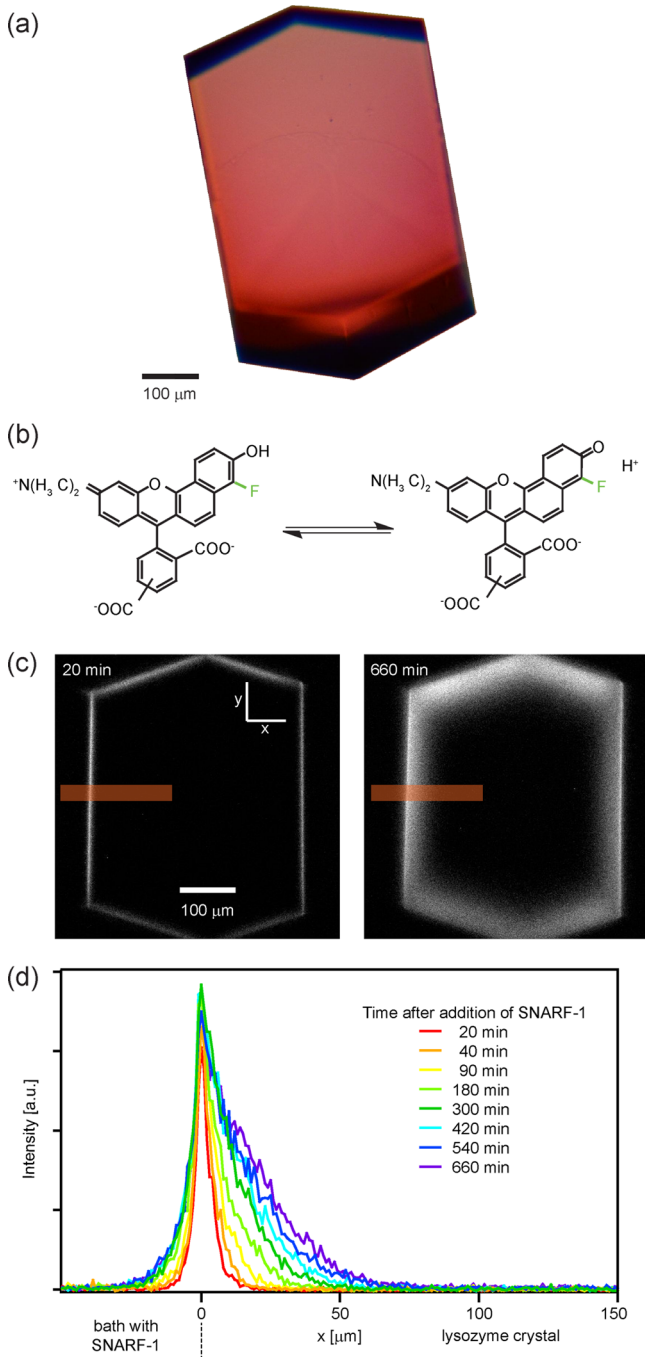


**Figure 1.** Lysozyme crystal labeled in a  $100 \mu\text{M}$  SNARF-1 bath accumulated the dye 275-fold and showed intense red color in transmitted light (a). The crystal is wedge-shaped and thinner at the top of the image. Such strong labeling should not be used for pH measurements to avoid fluorescence reabsorption, fluorescence resonance energy transfer, or pH buffering by the dye. The structure of SNARF-1 and its fluorinated and therefore  $\text{pK}_a$ -shifted derivative SNARF-4F (green) (b). The progress of labeling a crystal in a  $0.5 \mu\text{M}$  SNARF-1 bath solution was imaged with two-photon microscopy (c). Images show the crystal 20 and 660 min after addition of dye. Traces averaged from the shaded areas in part c show the diffusion of dye into the crystal (d).

in our experiments. A second explanation is that the accessible space for the dye is less than the 36% of water-filled volume. Water molecules tightly bound to the protein surface could be the reason for this. A 7.4-fold lower  $A_{\text{open}}/A_{\text{total}}$  ratio of 0.05

would fulfill the equation. With this change of the ratio, also the SNARF-1 concentration in the channels would increase 7.4-fold while the diffusion coefficient of SNARF-1 remains  $400 \mu\text{m}^2/\text{s}$ . The actual process might be a combination of both described processes.

In general, the labeling experiments reveal that it is very important to add only a low concentration of SNARF-1 to the crystals as otherwise, due to the accumulation, interactions like reabsorption of fluorescence or Förster resonance energy transfer (FRET) might occur. The absorption and emission spectra<sup>11</sup> suggest that the orange fluorescence of the protonated SNARF-1 or SNARF-4F molecule can excite the corresponding deprotonated molecules. This will shift the ratio and thus cause an artificial increase in the measured pH. Therefore, we reduced the dye concentration 200 times for pH imaging compared to the above labeling experiments. Crystals used for pH imaging did not show any color in transmitted light.

We were able to label lysozyme crystals with SNARF-1 and also with SNARF-4F (Figure 1b) to study a pH range of pH 5.5 to 8.0. We expect that structurally similar pH-sensitive dyes can also be used, allowing pH determination in an even wider range.<sup>11</sup> Additionally, we expect that also other ion sensitive synthetic fluorescent probes, for example, for  $\text{Ca}^{2+}$ ,  $\text{Mg}^{2+}$ ,  $\text{Zn}^{2+}$ ,  $\text{Na}^+$ ,  $\text{Al}^{3+}$ ,  $\text{Cu}^{2+}$ ,  $\text{Cu}^+$ ,  $\text{Fe}^{2+}$ ,  $\text{Hg}^{2+}$ ,  $\text{Pb}^{2+}$ ,  $\text{Cd}^{2+}$ ,  $\text{Zn}^{2+}$ ,  $\text{La}^{3+}$ , and  $\text{Ni}^{2+}$ , can be used to measure respective concentrations in protein crystal channels if the channels are wide enough for the dye to fit.

**SNARF-1/Lysozyme Crystal Interaction.** To examine any possible detrimental influence of dye on the morphology of the crystal, X-ray diffraction experiments were done using a dye-soaked lysozyme crystal and the high-resolution electron density was determined. The analysis of the difference electron density, obtained by comparing relevant data from the protein data bank of the Brookhaven National Laboratory and our structural data gained from a dye-soaked protein crystal, revealed a structural refinement factor of  $R = 0.16$ . This value lies below the threshold value of  $R = 0.2$  which is typical for a good structural refinement of proteins. Hence, we conclude that SNARF-1, even at concentrations 200-fold higher than those used for the fluorescence experiments, did not disturb the lysozyme crystal structure.

To test if SNARF-1 binds to lysozyme, gel electrophoresis experiments were conducted. The obvious separation of SNARF-1 from the protein excluded binding between protein and dye in solution.

Molecular interactions between dye and protein change the fluorescence characteristics due to altered energy levels of electron orbitals. When comparing the emission maxima of dye in bath solution, in the crystal, and in the literature,<sup>11</sup> no spectral shift was found (see below “Spectral Characteristics of SNARF-1 in Lysozyme Crystals”), indicating no dye/protein interactions. This confirms previous studies which show no SNARF-1/protein interactions in cells.<sup>18</sup>

Finally, we verified by destaining of the crystal that the dye remains chemically unbound in the crystal. A destaining time constant for crystals with a typical size of  $200 \times 200 \times 200 \mu\text{m}^3$  was  $\tau = 13 \pm 3 \text{ h}$ . We also did not find residual labeling which would indicate trapped dye molecules. Thus, the dye is not bound to the crystal but diffuses slow enough for stable measurements.

Therefore, the molecular pH probe SNARF-1 fulfills the essential requirements of a useful probe for pH measurements within a protein crystal.

**Spectral Characteristics of SNARF-1 in Lysozyme Crystals.** For pH measurements within the crystal, two-dimensional fluorescence spectra of a SNARF-1 loaded lysozyme crystal were measured 4 h after titration to a pH between 7.0 and 8.0 (Figure 2). On our setup, the

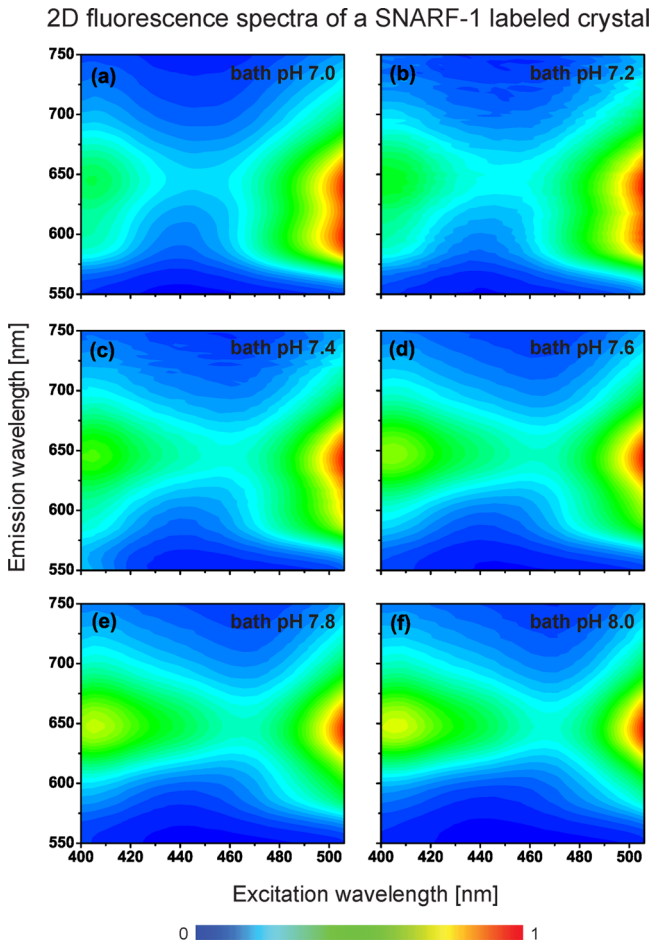


**Figure 2.** Two-dimensional fluorescence spectra of SNARF-1-dyed lysozyme crystals recorded at a pH of 7.0 (a), 7.2 (b), 7.4 (c), 7.6 (d), 7.8 (e), and 8.0 (f). With increasing pH, the emission of the protonated state at  $\lambda_a = 595$  nm decreases, while the emission of the deprotonated state at  $\lambda_b = 640$  nm increases. This pH-dependent dual-emission characteristic holds for the first excited electronic state (S1, excitation between 460 and 505 nm) but also for the second (S2, excitation between 400 and 450 nm).

measurement spot size can be adjusted by the field aperture down to a circle with  $5\text{ }\mu\text{m}$  diameter. The aperture was adjusted to illuminate the whole crystal so that the measured parameters are average parameters of the whole crystal.

The two emission maxima did not show a spectral shift compared to the published spectra of dye solutions at  $\lambda_a = 595$  nm and  $\lambda_b = 640$  nm.<sup>11</sup> At pH 7.0 of the bath solution, the fluorescent dye inside the protein crystal exhibited comparably intense emission peaks at  $\lambda_a$  and  $\lambda_b$  in the first excitation band. At pH 8, the fluorescence spectra showed a complete shift to the higher wavelength corresponding to the deprotonated state of the pH probe.

To calibrate the pH measurement in the crystal, we compared the emission spectra of the crystal with the spectra of SNARF-1 in solution (Figure 3). We analyzed and compared the emission spectra in the first and second electronically

excited state of SNARF-1 at an excitation wavelength of  $\lambda_{S1} = 505$  nm (Figure 3a,b) and  $\lambda_{S2} = 420$  nm (Figure 3c,d) to examine the excitation wavelength dependence of the pH measurement.

At  $\lambda_{S1}$ , the spectral changes between pH 7.0 and 8.0 were much more pronounced than at the shorter excitation wavelength of  $\lambda_{S2}$ . As the fluorescence characteristics are expected to be independent of the excitation wavelength, we assume the ratio of absorption coefficient and/or quantum efficiency of the deprotonated and protonated state of SNARF-1 is lower at  $\lambda_{S2}$  than at  $\lambda_{S1}$  and so less favorable for pH measurements in the range 7.0–8.0. Therefore, we focused on the spectral fluorescence intensities taken at  $\lambda_{S1} = 505$  nm to extract the ratios of fluorescence intensities characteristic for the pH.

**Average pH in Lysozyme Crystals.** Figure 4 shows the intensity ratios  $I_b/I_a$  determined from the fluorescence intensities recorded at  $\lambda_b = 640$  nm and  $\lambda_a = 595$  nm of SNARF-1 in buffer solution and in the lysozyme crystal, respectively. The calibration and dye-in-crystal spectra were measured on the same setup and under the same conditions to avoid any methodical differences which could introduce systematic errors. We found that all pH values measured in the crystal were lower than the pH in the corresponding buffer and bath solution. In pH 7.0 and 8.0 bath solutions, we measured a pH shift averaged over the whole crystal of  $\Delta\text{pH} = -0.30 \pm 0.03$  ( $\pm 3\sigma$ ) and  $-0.31 \pm 0.03$ , respectively. This average pH difference corresponds to a 2-fold higher proton concentration in the crystal compared to the bath.

**Three-Dimensional Reconstruction of a Lysozyme Crystal with Two-Photon Microscopy.** Using two-photon microscopy, we reconstructed SNARF-1- and SNARF-4F-labeled crystals three-dimensionally and analyzed the spatial distribution of the dye inside the crystal (Figures 5a and 6a,c). In crystals with a surface perpendicular to the optical axis, we found homogeneous labeling (central part of crystal in Figure 6a,c). Crystal edges or nonperpendicular surfaces split, refracted, focused, or reflected the laser beam and thus caused a decrease or increase of fluorescence intensity. pH measurements are not affected by these intensity modulations, as they cancel out in ratiometric measurements (Figure 5b,c center): The excitation intensity in the focus is changing, but this affects both fluorescence channels in the same way. The wavelength-dependent refraction of the emitted light can be neglected, as the difference in deflection is small between orange and red.

**Spatially and Temporally Resolved pH Change in a Lysozyme Crystal.** To test how fast the pH adjusts in a lysozyme crystal, we imaged a crystal before and repeatedly after a bath pH change from pH 6 to pH 7.5 (Figure 5). At buffer pH 6.0, the optical detected pH in the crystal was below pH 6.0 (Figure 5d,e). At the surface, the pH was higher than in the core. The pH decreased in the outermost  $30\text{ }\mu\text{m}$  from the surface and then remained constant. After the bath pH changed to pH 7.5, the pH at the surface of the crystal increased to pH 7.25 already during the first 10 min (Figure 5d,e). Exceptions were the (110) face of the crystal which laid on the glass coverslip and a crystal face of higher order on the opposite side of the (110) face (Figure 5d, second cross section). The core remained at unchanged pH for more than 20 min and only after 60 min reached equilibrium at pH 7.1 (Figure 5d,e). Because of the different buffers with different  $pK_a$ 's and the unknown concentrations of acetate and Tris buffer in the crystal, the proton diffusion cannot be easily deduced from the pH change.

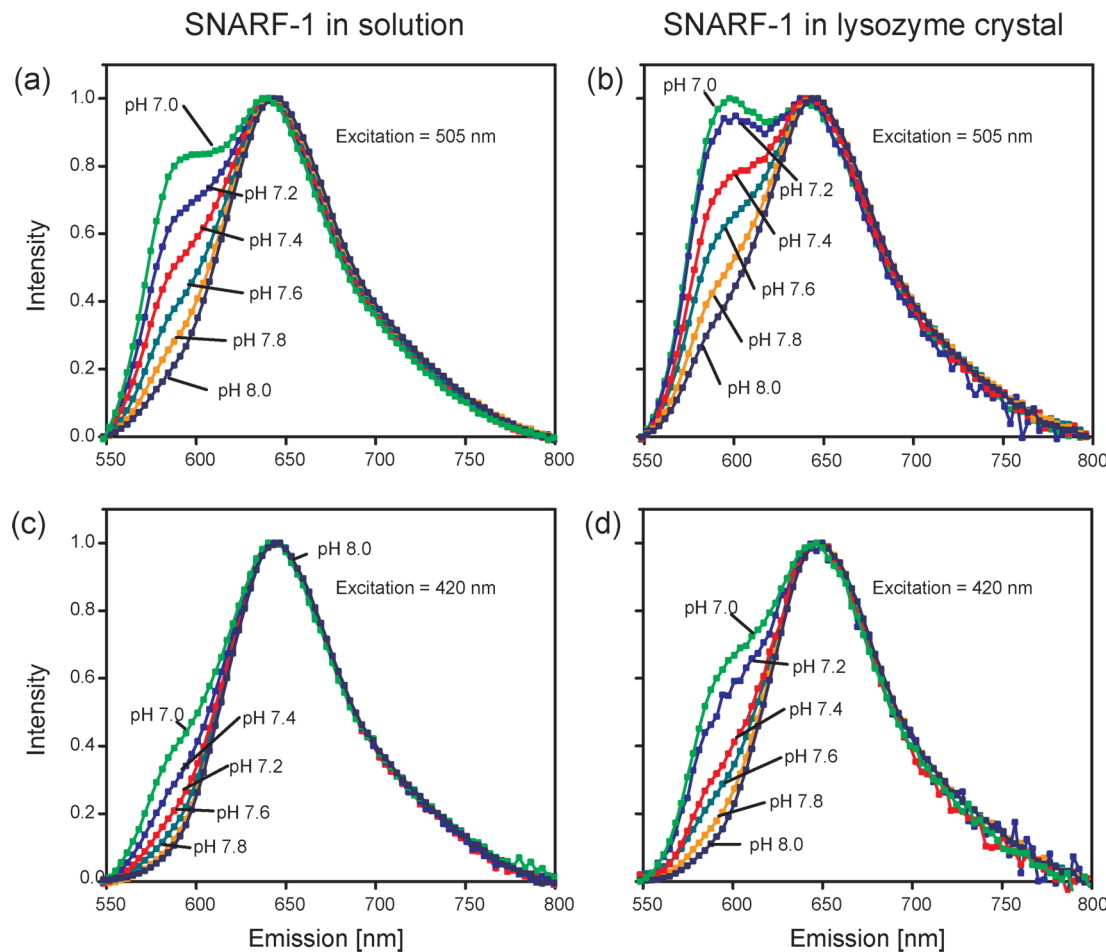


**Figure 3.** Emission spectra of SNARF-1, excited at 505 and 420 nm, showing the pH-dependent fluorescence of the buffered calibration solution (a, c) and the labeled crystal (b, d) for a bath pH ranging from 7.0 to 8.0. SNARF-1 exhibits more pronounced dual emission in the S1 state (a, b) than in S2 (c, d). All spectra were normalized to the emission maximum at  $\lambda_b = 640$  nm.

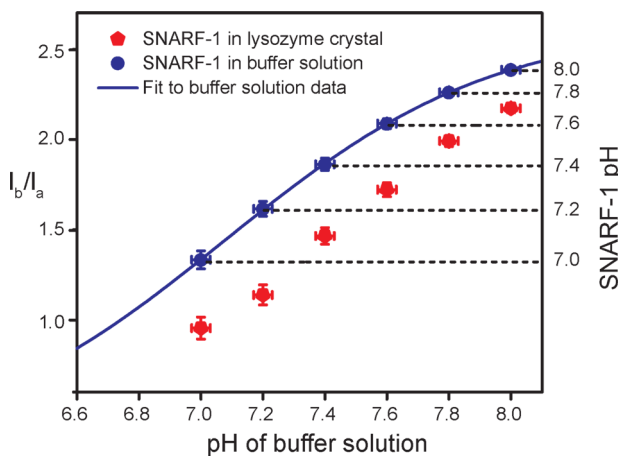


**Figure 4.** The average pH in the protein crystal is determined by relating the fluorescence ratio  $I_b/I_a$  measured at  $\lambda_a = 595$  nm (protonated dye) and  $\lambda_b = 640$  nm (deprotonated dye) of the crystal (red) ( $\pm 3\sigma$  error bars) with a buffered calibration solution (blue). The fit to the intensity ratio of the dye solution is used to calibrate the spectrometric pH measurement (right scale).

However, it is possible to get an estimate for the lower limit of the proton diffusion coefficient. We analyzed the proton concentration curve and found a lower limit of the proton diffusion coefficient of  $1 \mu\text{m}^2/\text{s}$  which is as expected

significantly slower than the long-range proton diffusion coefficient in lysozyme crystals reported before ( $\sim 36 \mu\text{m}^2/\text{s}$ ).<sup>6</sup>

**Spatially Resolved pH Equilibrium in a Lysozyme Crystal.** For the equilibrium pH at different buffer pH levels (Figure 6), we repeatedly changed the bath and waited for 90 min before imaging. We used SNARF-1 for the range of pH 7.0–8.0 (Figure 6a,b) in a Tris-buffered bath and SNARF-4F for the range of pH 5.5–6.5 (Figure 6c,d) in an acetate buffered bath.

With SNARF-1, the core of the crystal remained at  $\Delta\text{pH} = -1.0, -0.9$ , and  $-0.8$  lower pH than the bath pH of 7.0, 7.5, and 8.0, respectively. The pH difference was larger than in the example of Figure 5, most probably because of the larger crystal size (1.6 times in the  $x$  direction). From the core toward the surface of the crystal, the pH increased and approached the bath pH. This increase of pH toward the surface is another important validation of the method: If the pH shift would be caused by the molecular environment,<sup>21</sup> a step function would be expected at the crystal surface but not a steady decrease toward the core of the crystal.

We also tested a second dye, SNARF-4F, to measure the pH in a lower pH range and to confirm the findings with SNARF-1. With SNARF-4F, we found a similar negative pH shift of  $\Delta\text{pH} = -0.4, -0.5$ , and  $-0.7$  at a bath pH of 5.5, 6.0, and 6.5. In contrast to the SNARF-1 measurements, the pH in the crystal was constant. The reason for this might be that the experiments

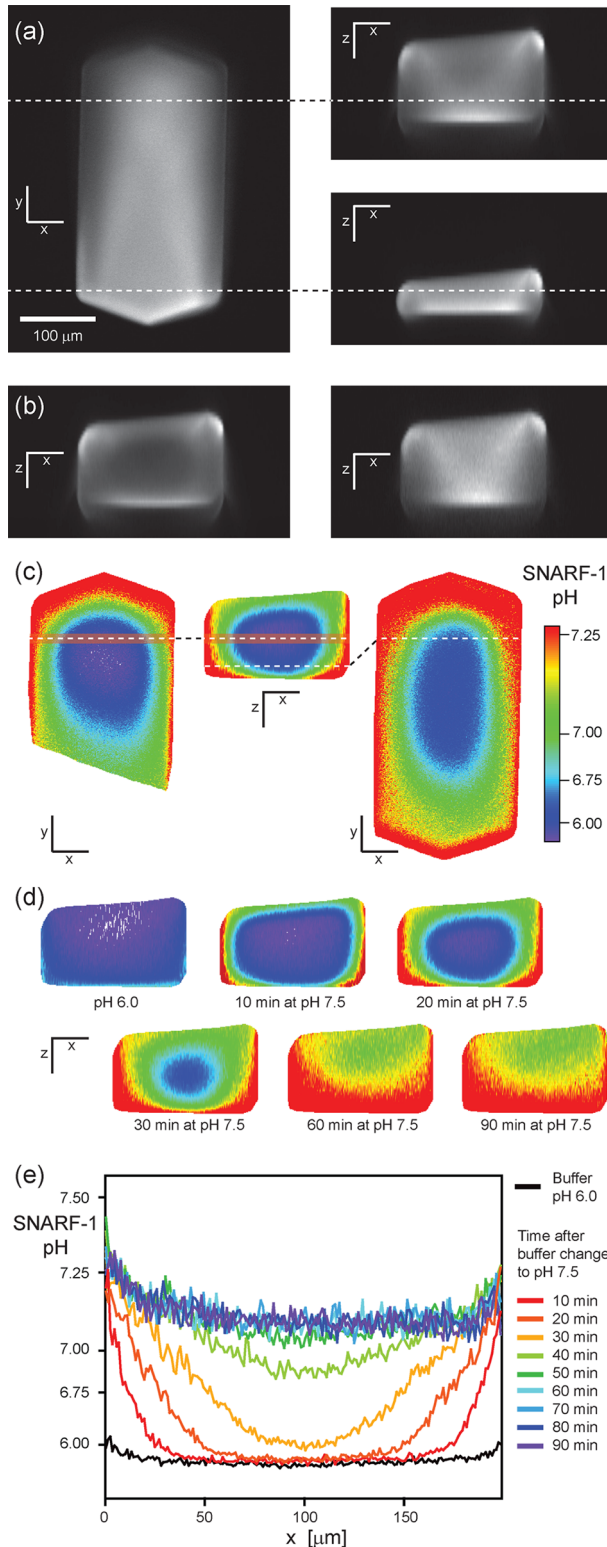


Figure 5. continued

min after raising the pH of the bath. Color code shows the pH calibration. Ratiometric  $x-z$  planes illustrate the progress of the pH change in the crystal (c). Traces (d) averaged from the orange shaded volume in part c show the pH every 10 min. The (110) face of the crystal is in the  $x-y$  plane.

were done in acetate buffer without change to Tris buffer as with the SNARF-1 experiments.

It is an important factor for the validation of the method that both dyes indicate a pH shift in a similar range.

The crystals in Figure 6b and d dissolved slightly and thus shrank 6 and 9% in the  $x$  direction during the procedure of imaging and buffer change, respectively. This might have been caused by the low but nonzero solubility of lysozyme in 1.2 M NaCl. We tested this hypothesis by saturating the bath solutions with lysozyme and were able to block the shrinkage.

**Proposed Mechanism Underlying the pH Shift in the Crystal.** If we consider an infinite proton buffered bath in contact with a finite buffered system and free ion exchange between bath and system, at equilibrium, the finite system is expected to adapt the pH of the bath. In our system of a lysozyme crystal in an almost infinite buffered bath, however, we find a decreased equilibrium pH in the tested range of bath pH from 5.5 to 8.0.

In previous studies, it was shown that protons have a reduced diffusion coefficient in the lysozyme crystal.<sup>6</sup> For this reason, we propose the same mechanism which we described for the dye diffusion before. Due to the conservation of mass at equilibrium, the flux of protons leaving and entering the crystal has to be equal.

$$\frac{A_{\text{open}}}{A_{\text{total}}} D_{\text{H}^+ \text{ bath}} [\text{H}^+]_{\text{bath}} = D_{\text{H}^+ \text{ crystal channel}} [\text{H}^+]_{\text{crystal channel}}$$

where  $D_{\text{H}^+}$  is the proton diffusion coefficient,  $[\text{H}^+]$  the proton concentration,  $A_{\text{total}}$  the surface area of the crystal, and  $A_{\text{open}}$  the surface of the crystal where protons can enter. The surface ratio  $A_{\text{open}}/A_{\text{total}}$  equals in a first approximation the relative water content of a crystal which, in the case of lysozyme, is 0.36.<sup>1,7</sup> In this model, the crystal symmetries and orientation of water-filled channels are not taken into account. Also, the effect of crystal size on the pH in the core needs further investigation. In the time course experiment, we found a lower limit of the proton diffusion coefficient of  $1 \mu\text{m}^2/\text{s}$ . A previous study found a diffusion coefficient for protons undergoing a diffusion motion confined within a sphere of  $390 \mu\text{m}^2/\text{s}$  and for protons undergoing a simple translation of  $36 \mu\text{m}^2/\text{s}$ .<sup>6</sup> Regarding the diffusion coefficient of protons in buffered saline of the bath, it is expected from previous studies that on one hand the diffusion is slowed down because of the high ionic strength<sup>27</sup> and that on the other hand the buffering improves the proton mobility.<sup>28,29</sup> Diffusion coefficients for protons in 1.4 M NaCl solutions at 25 °C were reported to be  $D_{\text{H}^+ \text{ crystal}} = 6552 \mu\text{m}^2/\text{s}$ .<sup>30</sup> If we use  $D_{\text{H}^+ \text{ crystal}} = 36 \mu\text{m}^2/\text{s}$ ,  $A_{\text{open}}/A_{\text{total}} = 0.36$ , and  $[\text{H}^+]_{\text{crystal channel}}/[\text{H}^+]_{\text{bath}} = 5$ , the above equation predicts  $D_{\text{H}^+ \text{ bath}} = 500 \mu\text{m}^2/\text{s}$ . A reduction of  $A_{\text{open}}/A_{\text{total}}$  to the same value as for the dye diffusion, which is 0.05, results in  $D_{\text{H}^+ \text{ bath}} = 3700 \mu\text{m}^2/\text{s}$ . Therefore, there is still a discrepancy between the experimental results and the first approximation of the model which needs further investigation, but the model can explain the order of magnitude of the pH shift. As the pH buffer

**Figure 5.** A SNARF-1-labeled crystal three-dimensionally reconstructed by two-photon microscopy (a). The wedge-shaped crystal is shown in the  $x-y$  imaging plane (left) and two reconstructed  $x-z$  planes (right) at the indicated locations (dashed lines). The bath solution of the crystal was changed from pH 6.0 to 7.5, and the crystal was subsequently imaged every 10 min with two-channel detection in the red (b, left) and orange (b, right) wavelength band to analyze the evolution of the pH change with time. The ratio of the red and orange channel  $x-z$  images of part b is shown in (c, center) as well as two  $x-y$  planes (c, left and right). The ratiometric images (c) were taken 20

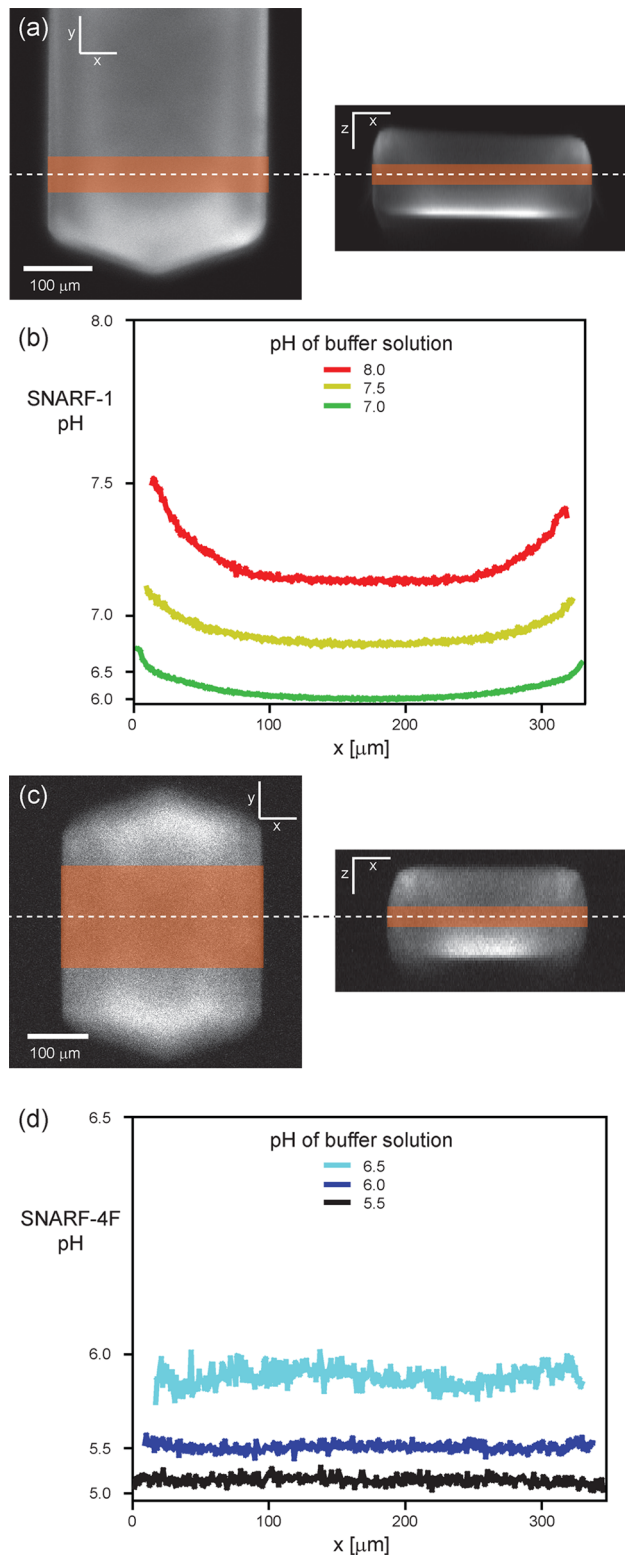


**Figure 6.** Two-photon images of a SNARF-1 (a) and a SNARF-4F (c) labeled crystal at pH equilibrium in the  $x-y$  (left) and  $x-z$  (right) imaging plane. Orange shade (a, c) indicates volume from which the equilibrium pH traces at different buffer pH (b, d) in the  $x$  direction were averaged. The (110) face of both crystals is in the  $x-y$  plane.

capacity of the system modulates the proton diffusion, the pH shift at different bath pH is not expected to be constant.<sup>28,29</sup> Also, the increase of the pH toward the surface in Tris buffered bath solutions can be explained by this. Tris slowly diffuses into

the crystal, increases the diffusion coefficient of protons close to the surface, and by this reduces the pH difference between crystal core and bath.

## CONCLUSIONS

We propose in this paper that the channels of the lysozyme crystal accumulate dye and protons as a result of a slower diffusion coefficient in the channels compared to the bath. As proton diffusion is expected to be hindered in all channels of protein crystals, every protein crystal pH should be lower than the bath pH in a proton-dominated pH range. We predict that at higher pH the proton diffusion will be in competition with  $\text{OH}^-$  diffusion, and then the  $\text{H}^+$  and  $\text{OH}^-$  concentrations and diffusion coefficients will determine the pH in the crystal channels in equilibrium.

We show that the pH in the channels of the lysozyme crystal can be raised to the physiological range by choosing a bath pH of 8.0. For other protein crystals, the pH shift has to be determined first. SNARF-1 should be used in a pH range between 6.0 and 8.5, while SNARF-4F is a useful probe between pH 5.0 and 7.0. The experiments are easy to set up and can be done not only on two-photon microscopes but also on confocal microscopes. The crystallographer who wants to know the pH of his crystals has to measure a ratiometric fluorescence calibration curve of the dye in solution and the ratiometric fluorescence of the dye soaked crystals under the same conditions (same setup, filters, and bath solutions). It is important to use low dye concentrations.

To what extent the protein structure in the crystal is altered by the change of the crystal pH remains to be tested and may vary for different proteins. The reason for this is that in the described method the second major parameter of protein conformation, the ionic strength, remains unchanged.

We expect that also many other fluorescent indicators can be used to study the concentration, distribution, and diffusion of different ions in protein crystals. Also for other ions the proposed model predicts that whenever the diffusion of an ion in the crystal is hindered an increased concentration compared to the bath is expected.

## AUTHOR INFORMATION

### Corresponding Author

\*E-mail: k.seemann@fz-juelich.de (K.M.S.); bkuhn@oist.jp (B.K.).

### Author Contributions

#K.M.S., R.K., and B.K. designed the experiments. K.M.S. and B.K. performed the spectrometric fluorescence measurements. K.M.S. and R.K. carried out X-ray diffraction experiments. B.K. built the 2P microscope and performed 2P imaging. K.M.S., R.K., U.J., and B.K. analyzed the data. K.M.S. and B.K. wrote the paper.

### Notes

The authors declare no competing financial interest.

## ACKNOWLEDGMENTS

The authors thank G. Ostertag, P. Fromherz, S. Willnow, E. Weinhold, and R. Huber for fruitful discussions and support during the early phase of the project, R. Huber for access to the Riga X-ray tube, and P. Fromherz for access to the microscope coupled spectrometer, both at the Max Planck Institute for Biochemistry, Martinsried.

**■ REFERENCES**

- (1) Blake, C. C.; Koenig, D. F.; Mair, G. A.; North, A. C.; Phillips, D. C.; Sarma, V. R. *Nature* **1965**, *206*, 757.
- (2) Bieri, O.; Kieffhaber, T. *J. Mol. Biol.* **2001**, *310*, 919.
- (3) Kieffhaber, T. *Proc. Natl. Acad. Sci. U.S.A.* **1995**, *92*, 9029.
- (4) Segel, D. J.; Bachmann, A.; Hofrichter, J.; Hodgson, K. O.; Doniach, S.; Kieffhaber, T. *J. Mol. Biol.* **1999**, *288*, 489.
- (5) Kuehner, D. E.; Engmann, J.; Fergg, F.; Wernick, M.; Blanch, H. W.; Prausnitz, J. M. *J. Phys. Chem. B* **1999**, *103*, 1368.
- (6) Bon, C.; Dianoux, A. J.; Ferrand, M.; Lehmann, M. S. *Biophys. J.* **2002**, *83*, 1578.
- (7) Morozov, V. N.; Kachalova, G. S.; Evtodienko, V. U.; Lanina, N. F.; Morozova, T. Y. *Eur. Biophys. J.* **1995**, *24*, 93.
- (8) Llopis, J.; McCaffery, J. M.; Miyawaki, A.; Farquhar, M. G.; Tsien, R. Y. *Proc. Natl. Acad. Sci. U.S.A.* **1998**, *95*, 6803.
- (9) Ohkuma, S.; Poole, B. *Proc. Natl. Acad. Sci. U.S.A.* **1978**, *75*, 3327.
- (10) Han, J. Y.; Burgess, K. *Chem. Rev.* **2010**, *110*, 2709.
- (11) Whitaker, J. E.; Haugland, R. P.; Prendergast, F. G. *Anal. Biochem.* **1991**, *194*, 330.
- (12) Liu, J.; Diwu, Z.; Leung, W. Y. *Bioorg. Med. Chem. Lett.* **2001**, *11*, 2903.
- (13) Buckler, K. J.; Vaughan-Jones, R. D. *Pflügers Arch.* **1990**, *417*, 234.
- (14) Boyer, M. J.; Hedley, D. W. *Methods Cell Biol.* **1994**, *41*, 135.
- (15) Bassnett, S.; Reinisch, L.; Beebe, D. C. *Am. J. Physiol.* **1990**, *258*, C171.
- (16) Ramshesh, V. K.; Lemasters, J. J. *Methods Mol. Biol.* **2012**, *810*, 243.
- (17) Hight, M. R.; Nolting, D. D.; McKinley, E. T.; Lander, A. D.; Wyatt, S. K.; Gonyea, M.; Zhao, P.; Manning, H. C. *J. Biomed. Opt.* **2011**, *16*, 016007.
- (18) Yassine, M.; Salmon, J. M.; Vigo, J.; Viallet, P. *J. Photochem. Photobiol., B* **1997**, *37*, 18.
- (19) Owen, S. O.; Carango, P.; Grammer, S.; Bobyock, S.; Leeper, D. B. *J. Fluoresc.* **1992**, *2*, 75.
- (20) Opitz, N.; Merten, E.; Acker, H. *Pflügers Arch.* **1994**, *427*, 332.
- (21) Fernandez, M. S.; Fromherz, P. *J. Phys. Chem.* **1977**, *81*, 1755.
- (22) Denk, W.; Strickler, J. H.; Webb, W. W. *Science* **1990**, *248*, 73.
- (23) Theer, P.; Kuhn, B.; Keusters, D.; Denk, W. Two-photon microscopy and imaging. In *Encyclopedia of molecular cell biology and molecular medicine*, 2nd ed.; Meyer, R. A., Ed.; Wiley-VCH Verlag: Weinheim, Germany, 20004; Vol. 1S, p 61.
- (24) Kuhn, B.; Fromherz, P. *J. Phys. Chem. B* **2003**, *107*, 7903.
- (25) Pologruto, T. A.; Sabatini, B. L.; Svoboda, K. *Biomed. Eng.* **2003**, *2*, 13.
- (26) Gendron, P. O.; Avaltroni, F.; Wilkinson, K. J. *J. Fluoresc.* **2008**, *18*, 1093.
- (27) Agmon, N.; Goldberg, S. Y.; Huppert, D. *J. Mol. Liq.* **1995**, *64*, 161.
- (28) Engasser, J. M.; Horvath, C. *Biochim. Biophys. Acta* **1974**, *358*, 178.
- (29) Engasser, J. M.; Horvath, C. *Physiol. Chem. Phys.* **1974**, *6*, 541.
- (30) Woolf, L. A. *J. Phys. Chem.* **1960**, *64*, 481.